Published in final edited form as:
Leukemia. 2016 June ; 30(6): 1388–1398. doi:10.1038/leu.2016.29.

DNMT3A^{R882H} mutant and *Tet2* inactivation cooperate in the deregulation of DNA methylation control to induce lymphoid malignancies in mice

Laurianne Scourzic[1,2,3,4], **Lucile Couronné**[1,2,3,4], **Marianne T. Pedersen**[5,6], **Véronique Della Valle**[1,2,3,4], **M'boyba Diop**[1,2,3,4], **Elena Mylonas**[1,2,3,4], **Julien Calvo**[2,3,7,8], **Enguerran Mouly**[1,2,3,4], **Cécile K. Lopez**[1,3,4], **Nadine Martin**[9,10], **Michaëla Fontenay**[11,12], **Ambre Bender**[13], **Sylvain Guibert**[13], **Patrice Dubreuil**[14,15], **Philippe Dessen**[1,2,3,4], **Nathalie Droin**[1,2,3,4], **Françoise Pflumio**[2,3,7,8], **Michael Weber**[13], **Philippe Gaulard**[9,10,16], **Kristian Helin**[5,6,17], **Thomas Mercher**[1,3,4], and **Olivier A. Bernard**[1,2,3,4]

[1]INSERM U1170, 94805 Villejuif, France

[2]Equipe labellisée Ligue Nationale Contre le Cancer, Paris, France

[3]Université Paris-Sud, 91405 Orsay, France

[4]Gustave Roussy, 94805 Villejuif, France

[5]Biotech Research and Innovation Centre (BRIC), 2200 Copenhagen, Denmark

[6]Centre for Epigenetics, 2200 Copenhagen, Denmark

[7]INSERM U967, Fontenay-aux-Roses, France

[8]CEA, DSV-IRCM-SCSR-LSHL, Fontenay-aux-Roses, France

[9]INSERM U955, Créteil, France

[10]Université Paris-Est, 94028 Créteil, France

[11]Département d'Immuno-Hématologie, Hôpital Cochin, 75014 Paris, France

[12]INSERM U1016, Centre national de la recherche scientifique (CNRS) UMR 8104, Institut Cochin, 75014 Paris, France

[13]CNRS, Université de Strasbourg, UMR7242, 67412 Illkirch, France

[14]INSERM U1068, CRCM, CNRS, université Aix-Marseille, 13273, Marseille, France

Correspondence to Olivier Bernard INSERM U1170, Gustave Roussy, 39 rue Camille Desmoulins, 94805 Villejuif, France olivier.bernard@inserm.fr, Tel: 33 1 42 11 42 33, Fax: 33 1 42 11 51 01.

AUTHORSHIP CONTRIBUTIONS

LS drafted the manuscript. LS and LC designed, performed and analyzed results. VDV, ElM, JC, EnM, CkL NM, ND, PG, MW, FP, MP, AB and KH performed experiments and analyzed data. MBD, PhD, MF, SG and PaD analyzed results. TM designed experiments, analyzed results and drafted the manuscript. OAB designed the project, experiments and wrote the manuscript.

CONFLICT OF INTEREST

The authors declare no conflict of interest

Supplementary Information is available at Leukemia's website

Europe PMC Funders Author Manuscripts

[15]Institut Paoli-Calmettes, Marseille, France

[16]Département de Pathologie, Hôpital Henri Mondor, 94028 Créteil, France

[17]The Danish Stem Cell Center, 2200 Copenhagen, Denmark

Abstract

TEN-ELEVEN-TRANSLOCATION-2 (*TET2*) and *DNA-METHYLTRANSFERASE-3A* (*DNMT3A*), both encoding proteins involved in regulating DNA methylation, are mutated in hematological malignancies affecting both myeloid and lymphoid lineages. We previously reported an association of *TET2* and *DNMT3A* mutations in progenitors of patients with angioimmunoblastic T-cell lymphomas (AITL). Here, we report on the cooperative effect of *Tet2*-inactivation and *DNMT3A* mutation affecting arginine 882 (*DNMT3A*^{R882H}) using a murine bone marrow transplantation assay. Five out of 18 primary recipients developed hematological malignancies with one mouse developing an AITL-like disease, 2 mice presenting acute myeloid leukemia (AML)-like and 2 others T cell acute lymphoblastic leukemia (T-ALL)-like diseases within 6 months following transplantation. Serial transplantations of *DNMT3A*^{R882H} *Tet2*$^{-/-}$ progenitors led to a differentiation bias toward the T-cell compartment, eventually leading to AITL-like disease in 9/12 serially transplanted recipients. Expression profiling suggested that *DNMT3A*^{R882H} *Tet2*$^{-/-}$ T-ALLs resemble those of *NOTCH1* mutant. Methylation analysis of *DNMT3A*^{R882H} *Tet2*$^{-/-}$ T-ALLs showed a global increase in DNA methylation affecting tumor suppressor genes and local hypomethylation affecting genes involved in the Notch pathway. Our data confirm the transformation potential of *DNMT3A*^{R882H} *Tet2*$^{-/-}$ progenitors and represent the first cooperative model in mice involving *Tet2*-inactivation driving lymphoid malignancies.

INTRODUCTION

DNA methylation of CpG dinucleotides is one of the major epigenetic marks in mammals and is known to play crucial roles in cellular processes including imprinting, gene expression regulation and control of differentiation. Mammalian enzymes catalyzing the conversion of cytosine to 5-methylcytosine (5-mC) by transferring a methyl group on the carbon 5 of cytosine belong to the DNA methyltransferase (DNMT) family including DNMT1, DNMT3A, DNMT3B and DNMT3L. Somatic heterozygous mutations in the *DNMT3A* gene have been reported in myeloid[1, 2] and lymphoid malignancies[3], and frequently target Arg882 (R882). The functional consequences of this mutant have been analyzed in murine embryonic stem (ES) cells, in which Dnmt3a^{R878H} inhibits wildtype (WT) Dnmt3a and Dnmt3b[4]. In human, the DNMT3A^{R882H} mutated protein presents as well a dominant-negative activity against DNMT3A^{WT} by preventing the active homotetramer formation[5]. *Dnmt3a*-null mice present a hematopoietic stem/progenitor cells (HSPC) expansion and differentiation bias toward B-cell compartment upon serial transplantations, those B-lymphocytes retaining high expression of HSC-associated genes[6].

Ten-Eleven-Translocation (TET) 2 catalyzes the conversion of 5-mC to 5-hydroxymethylcytosine (5-hmC) and may lead to active DNA demethylation. Loss of function mutations affecting *TET2* gene have been described in human hematological malignancies affecting both myeloid and lymphoid lineages[7-9]. Studies in *Tet2*-inactivated

mice revealed a cell-autonomous competitive advantage of hematopoietic progenitors followed by Chronic Myelomonocytic Leukemia (CMML) in a fraction of the animals[10]. This late malignant development in *Tet2*-inactivated context suggests that cooperative mutations are necessary for full-blown malignancy. Recently such cooperations have been experimentally demonstrated in myeloid transformations in mice[11-17].

We previously reported a significant co-occurrence of *TET2* and *DNMT3A* mutations in peripheral T-cell lymphoma (PTCL) patients; particularly frequent in angioimmunoblastic T-cell lymphoma (AITL)[3, 18, 19]. *TET2*-mutated PTCL show a follicular helper T cell (T_{fh}) signature and correlate with adverse outcome in patients[20].

Here, we explore the functional consequences of *TET2* and *DNMT3A* mutations cooperation in hematopoiesis using a bone marrow transplantation assay (BMT) in which mutant $DNMT3A^{R882H}$ is expressed in *Tet2*-inactivated ($Tet2^{-/-}$) HSPC. *Tet2* inactivation and $DNMT3A^{R882H}$ expression induced T-ALL or AML 6 months after transplantation. T-ALL is associated with hypermethylation and down-regulation of tumor suppressor genes and hypomethylation and up-regulation of *Notch1* oncogene. The majority of serially transplanted mice developed an AITL-like disease closely resembling the human disease. Our data constitutes the first cooperative murine model of T-cell malignancies involving *Tet2* inactivation.

METHODS

Plasmid construction

Full-length human $DNMT3A^{R882H}$, $NOTCH1^{L1601P\Delta P}$ and *TCL1A* cDNA were subcloned into MSCV-GFP backbone. Retroviral preparations and transduction were performed as previously published[21].

Murine bone marrow transplantation

Bone marrow transplantation using 3 months old C57BL/6 WT and $Tet2^{-/-}$ donors were performed as described previously[8] leading to *MSCV* $Tet2^{+/+}$, $DNMT3A^{R882H}$ $Tet2^{+/+}$, *MSCV* $Tet2^{-/-}$ (n=20), and $DNMT3A^{R882H}$ $Tet2^{-/-}$ (n=18) mice. For serial transplantation, HSPC were flow-sorted from whole marrow 16 weeks after transplantation, using GFP^+ Lin^- Kit^+ gating and engrafted with supplemented with 2.5×10^5 total marrow in lethally irradiated recipients (n=10). Animal experiments were approved by the Gustave Roussy animal care and use committees, according to ARRIVE guidelines.

Cell culture and western blotting

Culture of MO467, R152 and R338 cell lines, western blotting protocols and antibodies are described in Supplementary Methods.

Cell purification and cytometry

Total white blood cells from hematopoietic organs were stained in PBS supplemented with 2% FBS with fluorochrome-conjugated mouse antibodies against specific hematopoietic lineage markers. For the analysis of transplant-receiving mice, WBM was stained with

fluorochrome-conjugated mouse antibodies to discriminate cells derived from competitors and donors ($CD45.1^+$ and $CD45.2^+$ respectively) and GFP expression was used to precisely define donor-derived cells (GFP^+ $CD45.2^+$). Fluorochrome-conjugated mouse antibodies were obtained from Becton Dickinson (Streptavidin/PeCy5, CD117/PeCy7, CD45.1/PE, CD4/PE or PB, CD8/PeCy7 or APC, CD19/APC, B220/APCCy7, TCR_β/PE, CD279/BV421, CD11b/PerCP-Cy5.5, Annexin V/APC, Ki67/PE) and eBiosciences (CD117/APCCy7, Sca-1/APC, CD45.2/APC, Gr1/PE). Hoescht 33342 was obtained from Invitrogen. APC BrdU Flow kit (Becton Dickinson) was used according to the manufacturer's instruction. Cell sorting was performed either on a MoFlow (Beckman Coulter) or Influx (Becton Dickinson) cell sorter and analysis on a Canto II (Becton Dickinson). FACS data were analyzed by FlowJo Software (v8.8.7).

Methylation and Hydroxymethylation analyses by MeDIP and hMeDIP sequencing

5-mC and 5-hmC DNA immunoprecipitations of genomic DNA were performed as described[22]. 200-500 bp genomic DNA fragments were obtained using the bioruptor (Diagenode) and adaptor ligation was performed with the NEBNext DNA sample Prep Master Mix. One μg of adaptor ligated DNA was heat denatured and incubated with an IgG control antibody or with polyclonal 5-hmC[22] or monoclonal 5-mC (Eurogentec) antibody. Dynabeads (Invitrogen) were added before immunoprecipitation and elution of DNA was obtained with proteinase K digestion. PCR amplification of immunoprecipitated DNA was performed using index Illumina multiplex primers and single-end sequenced on HiSeq-2000. Reads were aligned to mouse genome mm10 with BWA aln (v0.7.3a) and peak calling assessed with the R package MEDIPS (v1.10.0). Differential analysis of (hydroxy)methylation was done with edgeR and annotation with HOMER (v4.7.2). Differentially (hydroxy)methylated regions with a p-value <0.001 and a FC>1.5 were considered as significant. HOMER was also used for transcription factor binding motif discovery.

Reduced Representation Bisulfite Sequencing (RRBS)

RRBS libraries were prepared as described previously[23] with minor modifications. Genomic DNA (50-200ng) was digested for 5 hours with MspI, end-repaired, A tailed and ligated with T4 DNA ligase (Fermentas) to methylated Illumina adaptors. 150-400 bp fragments were gel-purified, bisulfite treated (EpiTect Bisulfite kit, Qiagen) and RRBS libraries were amplified by 15 cycles of PCR with PfUTurbo Cx hotstar DNA polymerase (Agilent) and indexed PE Illumina primers. The libraries were paired-end sequenced (2×75bp) on a HiSeq-2000 to an average of 30 million pairs of reads per sample. Raw reads were cleaned with Trim Galore (v0.2.1) and aligned to the mm10 genome with BSMAP (v2.74). We identified DMRs with the eDMR algorithm from the methylKit R package with the following criteria: at least 3 CpGs, a difference in methylation greater than 20% and an adjusted p-value <0.01. DMRs were annotated using the RefSeq mm10 transcript annotation.

RNAseq

RNA was extracted with the AllPrep kit (Qiagen), quantified as above and checked with Bioanalyzer (Agilent). SureSelect Automated Strand Specific RNA Library Preparation Kit

was used according to manufacturer's instructions. Expression analysis was performed by counting the number of reads per gene using HTSeq-count and differential expression was assessed using the R package DESeq. P-values < 0.05 and −2 <FC> 2 were used as thresholds for differentially expressed genes.

ChIPseq

ChIP analyses were performed according to the MagnaChIP kit (Millipore). Briefly, 10×10^6 MO467 or R152 cells were prepared as previously published[24] with normal rabbit IgG (Millipore), H3K4me3 (Diagenode) and H3K27me3 (Millipore) antibodies. Adaptor-ligated libraries were prepared from 10ng of immunoprecipitated DNA using SPRIworks (Beckman Coulter). After indexed PCR amplification, the libraries were pooled and subjected to single-end sequencing. Reads were aligned to mouse genome mm10 with BWA aln (v0.7.5a) and peak calling assessed using MACS2 (v2.0.10.20131216) with a q-value cut-off <0.05. Annotation has been done with HOMER (v4.7.2).

Data access

(h)MeDIP, RRBS, RNAseq and ChIPseq data have been deposited at ArrayExpress under accession numbers E-MTAB-4157 to E-MTAB-4161.

Statistics

Data are depicted as mean ± s.e.m as precised. P-values were calculated with the two-tailed unpaired Student's *t* test. P-values for survival curves were calculated using a Log-rank (Mantel-Cox) test. All statistical analyses were performed with Prism software version 6.0 (GraphPad). The size of animal cohorts was based on our previous studies as well as published literature. Neither randomization, nor blinding was used since all animal experiments were performed with homogeneous strain, age, and similar variance.

RESULTS

Impairment of *DNMT3A^{R882H} Tet2$^{-/-}$* HSPCs differentiation *in vivo*

We performed BMT assays using *Tet2* wild type (*Tet2$^{+/+}$*) or *Tet2$^{-/-}$* murine HSPC, transduced with *DNMT3A^{R882H}*-expressing retroviruses. Monthly sampling of recipient mice revealed a mild growth advantage for *DNMT3A^{R882H} Tet2$^{-/-}$* cells over non-transduced *Tet2$^{-/-}$* cells, as shown by the constant increase of GFP$^+$ cells in recipients. In contrast, empty vector or *DNMT3A^{R882H}* expression alone did not confer growth advantage over untransduced cells in a *Tet2$^{+/+}$* context (figure 1A). Engrafted cells showed efficient contribution to mature T-, B- and myeloid cells (figure 1B) although myeloid cells expanded in *Tet2$^{-/-}$*, as compared to *Tet2$^{+/+}$* context. Contribution to the T-cell lineage was slightly decreased when *DNMT3A^{R882H}* was expressed as compared to MSCV in the *Tet2$^{-/-}$* context. The analysis of marrow and thymus of 3 mice per group 4 months after transplantation did not reveal significant difference in lineages proportions (figure 1C) nor in thymic population repartition (figure S1A). However, an increased proportion of Lin$^-$ Kit$^+$ (LK) and Lin$^-$ Sca$^+$ Kit$^+$ (LSK) cells was observed when *DNMT3A^{R882H}* is expressed (figure 1D), in keeping with previous reports showing increased contribution of *Dnmt3a*-inactivated cells to the stem/progenitor fraction[6].

Since *Dnmt3a*-inactivation has been shown to impair HSPC differentiation upon serial transplantation[6], we sorted GFP$^+$ LK progenitors of 3 *DNMT3A*^{R882H} *Tet2*$^{-/-}$ or *Tet2*$^{+/+}$ mice 16 weeks post-transplantation and serially transplanted them into 10 secondary mice. GFP$^+$ LK progenitors from 3 secondary mice were engrafted in 10 tertiary recipients. *DNMT3A*^{R882H} *Tet2*$^{-/-}$ cells showed efficient participation to mature blood cells in both secondary and tertiary experiments, indicating their self-renewal capacity, whereas *DNMT3A*^{R882H} *Tet2*$^{+/+}$ progenitors were progressively diluted (figure 1E). Detailed analyses showed that the contribution of the donor-derived cells to mature lineages differs between *Tet2* contexts in both secondary and tertiary transplantations (figure 1F). Expression of *DNMT3A*^{R882H} in *Tet2*$^{+/+}$ context induced an increase in the B-cell fraction, in keeping with the reported B-cell bias of *Dnmt3a*-inactivated HSPCs[6]. Expression of *DNMT3A*^{R882H} in *Tet2*$^{-/-}$ progenitors led to an expansion of the T-cell compartment in blood in both secondary and tertiary transplantations. However, *DNMT3A*^{R882H} *Tet2*$^{-/-}$ marrow examination did not show significant differences in lineage contribution in secondary transplant (figure 1G, left) while 3^{ary} transplants showed an accumulation of mature myeloid cells in marrow as compared with *DNMT3A*^{R882H} *Tet2*$^{+/+}$ mice (figure 1G, right). As expected for *Tet2*$^{-/-}$ cells, the proportion of *DNMT3A*^{R882H} *Tet2*$^{-/-}$ HSPC in the bone marrow was significantly higher, compared to *DNMT3A*^{R882H} *Tet2*$^{+/+}$ HSPC in secondary and tertiary transplanted recipients (figure 1H). No difference in thymic populations repartition between *DNMT3A*^{R882H} *Tet2*$^{-/-}$ and *DNMT3A*^{R882H} *Tet2*$^{+/+}$ secondary recipients was observed (figure S1B). Overall, these results indicate cooperation of the *DNMT3A*^{R882H} mutant with *Tet2*-inactivation leading to differential accumulation of *DNMT3A*^{R882H} *Tet2*$^{-/-}$ cells in hematopoietic organs, with myeloid cells primarily in the marrow and T-cells in the blood.

AITL-like development in *DNMT3A*^{R882H} *Tet2*$^{-/-}$ serially transplanted engrafted mice

During the course of the monitoring (10 to 16 months after transplantation), we sacrificed 4 (out of 6 secondary) and 5 (out of 6 tertiary) *DNMT3A*^{R882H} *Tet2*$^{-/-}$ mice, based on peripheral cytopenia and splenomegaly (Table 1). Analyses identified enlarged thymus, along with an expansion of the CD4$^+$ T-cell population in the thymus (figure 2A, left) and in all hematopoietic organs investigated (data not shown). Since human AITL is associated with high PD1 expression levels, we investigated its expression in *DNMT3A*^{R882H} *Tet2*$^{-/-}$ T-cell populations. Cell surface expression of PD1 was observed on GFP$^+$ CD4$^+$ cells in every tissue, including lymph nodes (figure 2A, right). Histopathological analysis of *DNMT3A*^{R882H} *Tet2*$^{-/-}$ symptomatic mice showed an infiltration of both the splenic white pulp and the liver by pleomorphic predominantly small to medium lymphoid cells accompanied by eosinophils, plasma cells and a few scattered larger cells resulting in alteration of the normal liver architecture with some focused perivascular infiltrations (figure 2B). The proliferation was essentially composed of CD3$^+$ and PD1$^+$ atypical T-cells, whereas CD79a staining highlighted recruitment of a few large B-lymphocytes in addition to the plasmocytes around T-cell infiltrates, therefore mimicking the pathological and phenotypic features of human AITL. The AITL phenotype was further underscored by the high expression of *Bcl6*, *Pdcd1*, *Cxcr5* and *Icos* genes[25, 26], in GFP$^+$ CD4$^+$ *DNMT3A*^{R882H} *Tet2*$^{-/-}$ cells as compared with normal *Tet2*$^{+/+}$ CD4$^+$ thymocytes (figure 2C).

Together, these data showed that 75% (9/12) of mice serially engrafted with *DNMT3A*^{R882H} *Tet2*$^{-/-}$ progenitors developed an AITL-like disease.

Mice transplanted with *DNMT3A*^{R882H} *Tet2*$^{-/-}$ HSPCs die prematurely and develop acute leukemias

We monitored disease development in primary recipients for one year. *Tet2*$^{+/+}$, *Tet2*$^{-/-}$ *and* *DNMT3A*^{R882H} *Tet2*$^{+/+}$ transplanted mice remained healthy throughout the period, whereas among the 18 *DNMT3A*^{R882H} *Tet2*$^{-/-}$ primary engrafted mice, 1 showed symptoms of AITL-like disease, 4 developed AML-like or T-ALL-like diseases, and were euthanized around 6 months post-engraftment (figure 3A and Table 1).

The 2 AML-like *DNMT3A*^{R882H} *Tet2*$^{-/-}$ mice exhibited hepatosplenomegaly and additional adenopathy (Table 1) consistent with 80% of Mac1^{+} Gr1^{+} Kit^{+} blastic myeloid population in the marrow (figure 3B, left). Secondary transplantation experiments performed with one of the AML sample also confirmed the malignant nature of the tumor (data not shown). Bone marrow from T-ALL-like *DNMT3A*^{R882H} *Tet2*$^{-/-}$ recipients exhibited more than 90% of abnormal GFP^{+} TCR$_{\beta}^{-}$ CD4^{+} CD8^{+} (double positive, DP) T-cells (figure 3B, right) which induced a similar T-ALL to transplanted recipients (figure S2A). Histopathological analysis showed alteration of the normal liver architecture with significant diffuse T-cell infiltration accompanied with focused perivascular infiltrations (figure S2B). These findings show that *DNMT3A*^{R882H} *Tet2*$^{-/-}$ progenitors are predisposed to both myeloid and lymphoid acute transformation *in vivo*.

Concomitant ablation of *Tet2* and overexpression of *DNMT3A*^{R882H} induce both global and local changes of 5-hmC and 5-mC epigenomic patterns

As the amount of material available from AITL-like mice was not sufficient, we then used *DNMT3A*^{R882H} *Tet2*$^{-/-}$ T-ALL models to investigate the mechanism underlying T-cell transformation using expression and methylation analyses. First, we performed transcriptome profiling of *DNMT3A*^{R882H} *Tet2*$^{-/-}$ T-ALL samples as well as T-ALL generated by BMT using known T-cell oncogenes: *TCL1A*[27] and *NOTCH1*$^{L1601P\Delta P}$ [28]. We used DP thymocytes from *Tet2*$^{-/-}$ and *Tet2*$^{+/+}$ mice as a reference (Table S1). Principal component analysis (PCA) based on global expression profiles identified 3 groups: 1- non-transformed *Tet2*$^{+/+}$ and *Tet2*$^{-/-}$ thymocytes, 2- TCL1A-induced T-ALLs and 3- *DNMT3A*^{R882H} *Tet2*$^{-/-}$ and *NOTCH*$^{L1601P\Delta P}$ *T-ALLs* (figure 3C, left). Differentially expressed genes between *DNMT3A*^{R882H} *Tet2*$^{-/-}$ and *Tet2*$^{+/+}$ thymocytes (Table S2) presented a marked overlap with known Notch pathway signatures (figure 3C, right), consistent with their clustering close to *NOTCH*$^{L1601P\Delta P}$ T-ALLs samples in the PCA.

Next, we compared DNA (hydroxy)methylation profiles between *DNMT3A*^{R882H} *Tet2*$^{-}$ T-ALLs, normal *Tet2*$^{-/-}$ thymocytes and other murine T-ALL samples (Table S1). Analyses of the combination of these samples allowed us to associate DNA (hydroxy)methylation changes to *Tet2*-inactivation, *DNMT3A*^{R882H} mutant or the cooperation of *Tet2*-inactivation and *DNMT3A*^{R882H} mutant. First, we analyzed hydroxymethylated and methylated DNA immunoprecipitation (hMeDIP and MeDIP, respectively) sequencing data (Table S3 and S4). Global hydroxymethylation is modified upon *Tet2*-inactivation, with almost all differentially

hydroxymethylated regions (DhMRs) being hypo-hydroxymethylated (figure 4A, top) and located in intergenic regions (figure S3A) as expected from the proposed function of *Tet2* in regulating enhancer activity[15, 29]. *Tet2*-inactivation was also associated with both hyper (n=1115) and hypo (n=90) differentially methylated regions (DMRs) (figure 4A, bottom). *DNMT3A*^{R882H} was not associated with hypo-DhMR but with some hyper-DhMRs, suggesting deregulation of the control of DNA hydroxymethylation. Both hyper and hypo DMRs were in greater numbers in *DNMT3A*^{R882H} than for *Tet2*-inactivation (2929 and 347 respectively), and frequently located in promoter regions for hypermethylation and in gene bodies for hypomethylation. The cooperation between those two previous conditions led to further deregulation of hydroxymethylation, some regions presenting less 5-hmC and some others more. The combination of both *Tet2*-inactivation and *DNMT3A*^{R882H} mutant presented almost the same number of DMR as compared with *DNMT3A*^{R882H} mutant alone, and did not markedly affect the repartition within the different genome annotations.

We then specifically analyzed the methylation at CpG islands (CpGi) regions through the mouse genome, by representing the coverage of reads obtained from hMeDIP and MeDIP (figure 4B). *Tet2*-inactivation was not associated with marked changes in 5-hmC or 5-mC contents whereas *DNMT3A*^{R882H} mutant expression was associated with higher 5-hmC levels and a strong increase in 5-mC. To obtain a more precise analysis of CpG methylation in *DNMT3A*^{R882H} *Tet2*$^{-/-}$ tumors, we performed Reduced Representation Bisulfite Sequencing (RRBS) sequencing on the same samples (Table S1). CpG methylation was increased in *DNMT3A*^{R882H} *Tet2*$^{-/-}$ samples with respect to other T-ALLs and *Tet2*$^{-/-}$ samples (figure S3B) and DMRs could be identified between samples (Table S5).

Specific transcriptional changes in tumoral *DNMT3A*^{R882H} *Tet2*$^{-/-}$ cells

Mean expression in *Tet2*$^{-/-}$ context of DMR-associated gene showed statistical differences only when DMRs were located within gene bodies, hyper-DMR being associated with higher expression and hypo-DMR with low expression (figure 5A). With *DNMT3A*^{R882H} mutant and *Tet2*-inactivation, hyper-DMRs were associated with lower gene expression, whereas hypo-DMRs were associated with higher expression.

We identified the genes that were statistically both hypermethylated and underexpressed in *DNMT3A*^{R882H} *Tet2*$^{-/-}$ cells (Figure 5B, top). 215 methylated CpG regions lie within 110 genes (Table S6). The sequences of the methylated CpG regions significantly showed DNA binding sequences of T-cell transcription factors, Thpok (Zbtb7b), Tcf1 and Tcf7 (figure S4A). Thpok is a key regulator of CD4 lymphocytes differentiation and upregulated in *DNMT3A*^{R882H} *Tet2*$^{-/-}$ cells as compared to *Tet2*$^{-/-}$ cells (data not shown). Tcf1 is a known tumor suppressor in T-cell transformation and a negative regulator of the Notch pathway[30-32]. Methylation of its target sites may mimic inactivation of the gene itself, as suggested here by the statistically significant down regulation of the β-catenin pathway (Figure 3C). Other tumor suppressor genes, known to be inactivated during hematopoietic transformation such as *Inpp4b*[33, 34] and *Tle4*[35] were among the 110 genes that both were hypermethylated and downregulated. An additional example is *Kdm5b*, which encodes a H3K4 demethylase (figure 5B, bottom).

Nine genes were statistically both hypomethylated and overexpressed (figure 5C, top and Table S7). Two of them, *Dtx1* and *Notch1* belong to the Notch pathway, which is essential for both normal and malignant T-cell differentiation. The hypomethylated region was located in the 3′ part (figure 5C, bottom) and was associated with *Notch1* overexpression in *DNMT3A*^{R882H} *Tet2*$^{-/-}$ tumor cells (figure S4B, top). Regarding *Dtx1* overexpression (figure S4B, bottom), the hypomethylated regions are also located in the 3′ part of the gene (figure S4C). To assess histone methylation marks associated with transcription activation or repression on *Notch1* and *Dtx1* loci, we performed ChIPseq on *DNMT3A*^{R882H} *Tet2*$^{-/-}$ (MO467) or *NOTCH1* $^{L1601P\Delta P}$ *Tet2*$^{+/+}$ (R152) murine T-ALL established cell lines (Table S1). Hypermethylated regions were associated with less H3K4me3 whereas hypomethylated regions were associated with H3K4me3 enrichment (figure 5C bottom and S4D).

Altogether, these results highlight a synergistic effect of *Tet2*$^{-/-}$ inactivation and *DNMT3A*^{R882H} overexpression on DNA methylation and gene expression, resulting in both down-regulation of tumor suppressor genes and up-regulation of oncogenes, including Notch pathway genes.

Notch dependency of tumor *DNMT3A*^{R882H} *Tet2*$^{-/-}$ cells

To functionally assess the role of the Notch pathway in this transformation process, we studied Notch-dependency of MO467 (*DNMT3A*^{R882H} *Tet2*$^{-/-}$) and R152 (*NOTCH1*$^{L1601P\Delta P}$ *Tet2*$^{+/+}$) established T-ALL cell lines. Activation of the Notch pathway in MO467 cells was confirmed by the presence of cleaved Notch1 proteins (figure 6A, left). Treatment of the cell lines with increasing amount of a γ-secretase inhibitor (GSI) led to decreased expression of the cleaved form of Notch1 (figure 6A, right) and decreased expression of known Notch1 target genes: such as *Hes1* and *Nrarp* (figure 6B). GSI treatment led to reduced viability/proliferation of *DNMT3A*^{R882H} *Tet2*$^{-/-}$ and *NOTCH1*$^{L1601P\Delta P}$ *Tet2*$^{+/+}$ cells but not of Ba/F3 cells (figure 6C) and was associated with an increased proportion of cells in G0/G1 and decrease of cells in S-phase in both *DNMT3A*^{R882H} *Tet2*$^{-/-}$ (figure S5A and 5B) and *NOTCH1*$^{L1601P\Delta P}$ *Tet2*$^{+/+}$ (data not shown) cell lines. We confirmed these results by treating R158 (*NOTCH1*$^{L1601P\Delta P}$ *Tet2*$^{-/-}$) and R467 (*DNMT3A*^{R882H} *Tet2*$^{-/-}$) primary cells cultured on MS5 and MS5-DL1 feeders, with another GSI (DAPT). *DNMT3A*^{R882H} *Tet2*$^{-/-}$ T-ALL cells proliferate in a Notch-dependent manner similarly to *NOTCH1*$^{L1601P\Delta P}$ *Tet2*$^{-/-}$ T-ALL cells, although they do not respond to classical Notch activation by DL1 ligand (figure S5C). Furthermore, an increased proportion of both apoptotic and G0/G1 *DNMT3A*^{R882H} *Tet2*$^{-/-}$ T-ALL cells is observed (figure S5D and E).

DISCUSSION

Here, we report that concomitant *DNMT3A*^{R882H} expression and loss of *Tet2* in mouse HSPC leads to both myeloid and lymphoid hematological malignancies. The AML-like disease developed by 10% of *DNMT3A*^{R882H} *Tet2*$^{-/-}$ mice is consistent with the recurrence of these mutations in human AML. The T-lymphoid diseases are more frequent, in keeping with the tight association between these mutations in human AITL. As the abnormal expansion of myeloid and T-cells is observed in different organs, marrow and blood

respectively, the microenvironment may play an important role in determining the amplified linages[36].

Our model represents the first cooperative murine model involving *Tet2*-inactivation in T-cell malignancies. In many aspects, these results are in accordance with *Dnmt3a*-null mice, which also develop both lymphoid and myeloid malignancies[37, 38]. We however did not observe B-cell malignancies, in keeping with the human situation: B-lymphoid malignancies essentially lack *DNMT3A* mutations in human.

The combination of *Tet2* loss and $DNMT3A^{R882H}$ expression resulted in high hydroxymethylation and methylation disorder. $DNMT3A^{R882H}$-associated hypermethylation, correlated with low expression of tumor suppressor loci and hypomethylation associated with high expression of oncogene. In our model, among the widespread DNA methylation aberrations, only few genes may have functional impact. This is exemplified by hypomethylation and overexpression of the *Notch1* and *Dtx1* genes, which results in the activation of the Notch pathway, a major oncogenic pathway in T-cell malignancies. Other abnormalities may sustain T-cell transformation, such as low expression of *Tcf1*, leading to the downregulation of the Wnt/β catenin pathway, as reported in a fraction of PTCL[39], together with methylation of the promoters of target genes. Overexpression of *Zbtb7b*, may be involved in the generation of hyper DMRs and cellular transformation[40].

Finally, the high frequency of DNMT3A mutations in adult T-ALL[41, 42] may be associated with *NOTCH1* hypomethylation causing high NOTCH1 expression during T-cell differentiation and subsequent occurrence of *NOTCH1* activation mutation to induce T-ALL. With age, our mouse model consistently develops an AITL-like disease, a lymphoma occurring in the elderly in human and for which only few mouse models exist[43, 44]. Given that AITL cells could not be engrafted aside from subsequent progenitors transplantation along with a decrease in the GFP^+ proportion, their isolation in sufficient number for functional analyses was precluded. The AITL phase is preceded by an expansion of the $CD4^+$ T-cell compartment, and associated with high *Notch1* and *Dtx1* expression (data not shown). The link between early expansion of the $CD4^+$ population and subsequent development of AITL-like disorder is at the moment speculative, but may rely on high expression *Thpok* and of *Notch1* during thymocytes differentiation. Recently, immunohistochemical analyses of human samples uncovered NOTCH1 activation in up to 38% of peripheral T cell lymphoma samples[45].

The relative low number of transformations observed in primary recipients likely reflects the insufficiency of *TET2* and *DNMT3A* mutations to drive full transformation. The observed bias toward T-cell abnormalities might be due to impaired methylation, which has been suggested to protect from lymphoid differentiation[46]. Serial transplantations might facilitate epigenetic drift, leading to Notch1 overexpression and $CD4^+$ T-cells accumulation.

Together, our data support the idea that Notch pathway activation represents an important survival signal for abnormal Tfh-cells. Interaction with B-lymphocyte and myeloid cells

might substitute for Notch survival signals required by these abnormal T_{fh}-cells[47] and/or for T-cells survival[48].

Supplementary Material

Refer to Web version on PubMed Central for supplementary material.

ACKNOWLEDGEMENTS

The authors thank members of the Bernard lab for helpful discussions, Julie Mouillaux for her involvement in this project, Patrick Gonin from the Gustave Roussy animal facility for excellent mouse care as well as Yann Lecluse and Philippe Rameau from the Gustave Roussy Flow Cytometry Core Facility. We also thank the Gustave Roussy Genomic Platform for high throughput sequencing. Work in the lab was supported by grants from INSERM, Institut National du Cancer (INCA), 2013-1-PL BIO-09, INCa-DGOS-INSERM 6043, Ligue Nationale Contre le Cancer (LNCC), Fondation pour la Recherche Médicale (FRM) and Association Laurette Fugain. The work in the lab of KH was supported by the Danish Cancer Society, the European Research Council (294666_DNAMET), the Danish National Research Foundation (DNRF82), and the Novo Nordisk Foundation. LS is supported by fellowships from Cancéropôle Ile de France and Fondation Association pour la recherche sur le Cancer (ARC).

REFERENCES

1. Ley TJ, Ding L, Walter MJ, McLellan MD, Lamprecht T, Larson DE, et al. DNMT3A mutations in acute myeloid leukemia. N Engl J Med. Dec 16; 2010 363(25):2424–2433. [PubMed: 21067377]
2. Yan XJ, Xu J, Gu ZH, Pan CM, Lu G, Shen Y, et al. Exome sequencing identifies somatic mutations of DNA methyltransferase gene DNMT3A in acute monocytic leukemia. Nature genetics. Apr; 2011 43(4):309–315. [PubMed: 21399634]
3. Couronne L, Bastard C, Bernard OA. TET2 and DNMT3A mutations in human T-cell lymphoma. N Engl J Med. Jan 5; 2012 366(1):95–96. [PubMed: 22216861]
4. Kim SJ, Zhao H, Hardikar S, Singh AK, Goodell MA, Chen T. A DNMT3A mutation common in AML exhibits dominant-negative effects in murine ES cells. Blood. Dec 12; 2013 122(25):4086–4089. [PubMed: 24167195]
5. Russler-Germain DA, Spencer DH, Young MA, Lamprecht TL, Miller CA, Fulton R, et al. The R882H DNMT3A mutation associated with AML dominantly inhibits wild-type DNMT3A by blocking its ability to form active tetramers. Cancer Cell. Apr 14; 2014 25(4):442–454. [PubMed: 24656771]
6. Challen GA, Sun D, Jeong M, Luo M, Jelinek J, Berg JS, et al. Dnmt3a is essential for hematopoietic stem cell differentiation. Nat Genet. Jan; 2012 44(1):23–31. [PubMed: 22138693]
7. Delhommeau F, Dupont S, Della Valle V, James C, Trannoy S, Masse A, et al. Mutation in TET2 in myeloid cancers. N Engl J Med. May 28; 2009 360(22):2289–2301. [PubMed: 19474426]
8. Quivoron C, Couronne L, Della Valle V, Lopez CK, Plo I, Wagner-Ballon O, et al. TET2 inactivation results in pleiotropic hematopoietic abnormalities in mouse and is a recurrent event during human lymphomagenesis. Cancer Cell. Jul 12; 2011 20(1):25–38. [PubMed: 21723201]
9. Langemeijer SM, Kuiper RP, Berends M, Knops R, Aslanyan MG, Massop M, et al. Acquired mutations in TET2 are common in myelodysplastic syndromes. Nature genetics. Jul; 2009 41(7):838–842. [PubMed: 19483684]
10. Scourzic L, Mouly E, Bernard OA. TET proteins and the control of cytosine demethylation in cancer. Genome Med. 2015; 7(1):9. [PubMed: 25632305]
11. Chen E, Schneider RK, Breyfogle LJ, Rosen EA, Poveromo L, Elf S, et al. Distinct effects of concomitant Jak2V617F expression and Tet2 loss in mice promote disease progression in myeloproliferative neoplasms. Blood. Jan 8; 2015 125(2):327–335. [PubMed: 25281607]
12. Kameda T, Shide K, Yamaji T, Kamiunten A, Sekine M, Taniguchi Y, et al. Loss of TET2 has dual roles in murine myeloproliferative neoplasms: disease sustainer and disease accelerator. Blood. Jan 8; 2015 125(2):304–315. [PubMed: 25395421]

13. Lobry C, Ntziachristos P, Ndiaye-Lobry D, Oh P, Cimmino L, Zhu N, et al. Notch pathway activation targets AML-initiating cell homeostasis and differentiation. J Exp Med. Feb 11; 2013 210(2):301–319. [PubMed: 23359070]
14. Muto T, Sashida G, Oshima M, Wendt GR, Mochizuki-Kashio M, Nagata Y, et al. Concurrent loss of Ezh2 and Tet2 cooperates in the pathogenesis of myelodysplastic disorders. J Exp Med. Nov 18; 2013 210(12):2627–2639. [PubMed: 24218139]
15. Rasmussen KD, Jia G, Johansen JV, Pedersen MT, Rapin N, Bagger FO, et al. Loss of TET2 in hematopoietic cells leads to DNA hypermethylation of active enhancers and induction of leukemogenesis. Genes Dev. May 1; 2015 29(9):910–922. [PubMed: 25886910]
16. Shih AH, Jiang Y, Meydan C, Shank K, Pandey S, Barreyro L, et al. Mutational cooperativity linked to combinatorial epigenetic gain of function in acute myeloid leukemia. Cancer Cell. Apr 13; 2015 27(4):502–515. [PubMed: 25873173]
17. Soucie E, Hanssens K, Mercher T, Georgin-Lavialle S, Damaj G, Livideanu C, et al. In aggressive forms of mastocytosis, TET2 loss cooperates with c-KITD816V to transform mast cells. Blood. Dec 6; 2012 120(24):4846–4849. [PubMed: 23074272]
18. Palomero T, Couronne L, Khiabanian H, Kim MY, Ambesi-Impiombato A, Perez-Garcia A, et al. Recurrent mutations in epigenetic regulators, RHOA and FYN kinase in peripheral T cell lymphomas. Nat Genet. Feb; 2014 46(2):166–170. [PubMed: 24413734]
19. Sakata-Yanagimoto M, Enami T, Yoshida K, Shiraishi Y, Ishii R, Miyake Y, et al. Somatic RHOA mutation in angioimmunoblastic T cell lymphoma. Nat Genet. Feb; 2014 46(2):171–175. [PubMed: 24413737]
20. Lemonnier F, Couronne L, Parrens M, Jais JP, Travert M, Lamant L, et al. Recurrent TET2 mutations in peripheral T-cell lymphomas correlate with TFH-like features and adverse clinical parameters. Blood. Aug 16; 2012 120(7):1466–1469. [PubMed: 22760778]
21. Malinge S, Ragu C, Della-Valle V, Pisani D, Constantinescu SN, Perez C, et al. Activating mutations in human acute megakaryoblastic leukemia. Blood. Nov 15; 2008 112(10):4220–4226. [PubMed: 18755984]
22. Williams K, Christensen J, Pedersen MT, Johansen JV, Cloos PA, Rappsilber J, et al. TET1 and hydroxymethylcytosine in transcription and DNA methylation fidelity. Nature. May 19; 2011 473(7347):343–348. [PubMed: 21490601]
23. Gu H, Smith ZD, Bock C, Boyle P, Gnirke A, Meissner A. Preparation of reduced representation bisulfite sequencing libraries for genome-scale DNA methylation profiling. Nat Protoc. Apr; 2011 6(4):468–481. [PubMed: 21412275]
24. Thiollier C, Lopez CK, Gerby B, Ignacimouttou C, Poglio S, Duffourd Y, et al. Characterization of novel genomic alterations and therapeutic approaches using acute megakaryoblastic leukemia xenograft models. J Exp Med. Oct 22; 2012 209(11):2017–2031. [PubMed: 23045605]
25. Crotty S. Follicular helper CD4 T cells (TFH). Annu Rev Immunol. 2011; 29:621–663. [PubMed: 21314428]
26. de Leval L, Rickman DS, Thielen C, Reynies A, Huang YL, Delsol G, et al. The gene expression profile of nodal peripheral T-cell lymphoma demonstrates a molecular link between angioimmunoblastic T-cell lymphoma (AITL) and follicular helper T (TFH) cells. Blood. Jun 1; 2007 109(11):4952–4963. [PubMed: 17284527]
27. Virgilio L, Lazzeri C, Bichi R, Nibu K, Narducci MG, Russo G, et al. Deregulated expression of TCL1 causes T cell leukemia in mice. Proc Natl Acad Sci U S A. Mar 31; 1998 95(7):3885–3889. [PubMed: 9520462]
28. Chiang MY, Xu L, Shestova O, Histen G, L'Heureux S, Romany C, et al. Leukemia-associated NOTCH1 alleles are weak tumor initiators but accelerate K-ras-initiated leukemia. J Clin Invest. Sep; 2008 118(9):3181–3194. [PubMed: 18677410]
29. Tsagaratou A, Aijo T, Lio CW, Yue X, Huang Y, Jacobsen SE, et al. Dissecting the dynamic changes of 5-hydroxymethylcytosine in T-cell development and differentiation. Proceedings of the National Academy of Sciences of the United States of America. Aug 12; 2014 111(32):E3306–3315. [PubMed: 25071199]

30. Steinke FC, Yu S, Zhou X, He B, Yang W, Zhou B, et al. TCF-1 and LEF-1 act upstream of Th-POK to promote the CD4(+) T cell fate and interact with Runx3 to silence Cd4 in CD8(+) T cells. Nat Immunol. Jul; 2014 15(7):646–656. [PubMed: 24836425]
31. Yu S, Xue HH. TCF-1 mediates repression of Notch pathway in T lineage-committed early thymocytes. Blood. May 9; 2013 121(19):4008–4009. [PubMed: 23660861]
32. Staal FJ, Clevers H. Tales of the unexpected: Tcf1 functions as a tumor suppressor for leukemias. Immunity. Nov 16; 2012 37(5):761–763. [PubMed: 23159221]
33. Li Chew C, Lunardi A, Gulluni F, Ruan DT, Chen M, Salmena L, et al. In Vivo Role of INPP4B in Tumor and Metastasis Suppression through Regulation of PI3K-AKT Signaling at Endosomes. Cancer Discov. Jul; 2015 5(7):740–751. [PubMed: 25883022]
34. Kofuji S, Kimura H, Nakanishi H, Nanjo H, Takasuga S, Liu H, et al. INPP4B Is a PtdIns(3,4,5)P3 Phosphatase That Can Act as a Tumor Suppressor. Cancer Discov. Jul; 2015 5(7):730–739. [PubMed: 25883023]
35. Greif PA, Eck SH, Konstandin NP, Benet-Pages A, Ksienzyk B, Dufour A, et al. Identification of recurring tumor-specific somatic mutations in acute myeloid leukemia by transcriptome sequencing. Leukemia. May; 2011 25(5):821–827. [PubMed: 21339757]
36. Wei J, Wunderlich M, Fox C, Alvarez S, Cigudosa JC, Wilhelm JS, et al. Microenvironment determines lineage fate in a human model of MLL-AF9 leukemia. Cancer cell. Jun; 2008 13(6): 483–495. [PubMed: 18538732]
37. Mayle A, Yang L, Rodriguez B, Zhou T, Chang E, Curry CV, et al. Dnmt3a loss predisposes murine hematopoietic stem cells to malignant transformation. Blood. Jan 22; 2015 125(4):629–638. [PubMed: 25416277]
38. Peters SL, Hlady RA, Opavska J, Klinkebiel D, Pirruccello SJ, Talmon GA, et al. Tumor suppressor functions of Dnmt3a and Dnmt3b in the prevention of malignant mouse lymphopoiesis. Leukemia. May; 2014 28(5):1138–1142. [PubMed: 24292811]
39. Dorfman DM, Greisman HA, Shahsafaei A. Loss of expression of the WNT/beta-catenin-signaling pathway transcription factors lymphoid enhancer factor-1 (LEF-1) and T cell factor-1 (TCF-1) in a subset of peripheral T cell lymphomas. Am J Pathol. May; 2003 162(5):1539–1544. [PubMed: 12707037]
40. Lee HO, He X, Mookerjee-Basu J, Zhongping D, Hua X, Nicolas E, et al. Disregulated expression of the transcription factor ThPOK during T-cell development leads to high incidence of T-cell lymphomas. Proc Natl Acad Sci U S A. Jun 23; 2015 112(25):7773–7778. [PubMed: 26056302]
41. Grossmann V, Haferlach C, Weissmann S, Roller A, Schindela S, Poetzinger F, et al. The molecular profile of adult T-cell acute lymphoblastic leukemia: mutations in RUNX1 and DNMT3A are associated with poor prognosis in T-ALL. Genes Chromosomes Cancer. Apr; 2013 52(4):410–422. [PubMed: 23341344]
42. Neumann M, Heesch S, Schlee C, Schwartz S, Gokbuget N, Hoelzer D, et al. Whole-exome sequencing in adult ETP-ALL reveals a high rate of DNMT3A mutations. Blood. Jun 6; 2013 121(23):4749–4752. [PubMed: 23603912]
43. Ellyard JI, Chia T, Rodriguez-Pinilla SM, Martin JL, Hu X, Navarro-Gonzalez M, et al. Heterozygosity for Roquinsan leads to angioimmunoblastic T-cell lymphoma-like tumors in mice. Blood. Jul 26; 2012 120(4):812–821. [PubMed: 22700722]
44. Muto H, Sakata-Yanagimoto M, Nagae G, Shiozawa Y, Miyake Y, Yoshida K, et al. Reduced TET2 function leads to T-cell lymphoma with follicular helper T-cell-like features in mice. Blood Cancer J. 2014; 4:e264. [PubMed: 25501021]
45. Kluk MJ, Ashworth T, Wang H, Knoechel B, Mason EF, Morgan EA, et al. Gauging NOTCH1 Activation in Cancer Using Immunohistochemistry. PLoS One. 2013; 8(6):e67306. [PubMed: 23825651]
46. Broske AM, Vockentanz L, Kharazi S, Huska MR, Mancini E, Scheller M, et al. DNA methylation protects hematopoietic stem cell multipotency from myeloerythroid restriction. Nat Genet. Nov; 2009 41(11):1207–1215. [PubMed: 19801979]
47. Auderset F, Schuster S, Fasnacht N, Coutaz M, Charmoy M, Koch U, et al. Notch signaling regulates follicular helper T cell differentiation. J Immunol. Sep 1; 2013 191(5):2344–2350. [PubMed: 23918982]

48. Fasnacht N, Huang HY, Koch U, Favre S, Auderset F, Chai Q, et al. Specific fibroblastic niches in secondary lymphoid organs orchestrate distinct Notch-regulated immune responses. J Exp Med. Oct 20; 2014 211(11):2265–2279. [PubMed: 25311507]

Europe PMC Funders Author Manuscripts

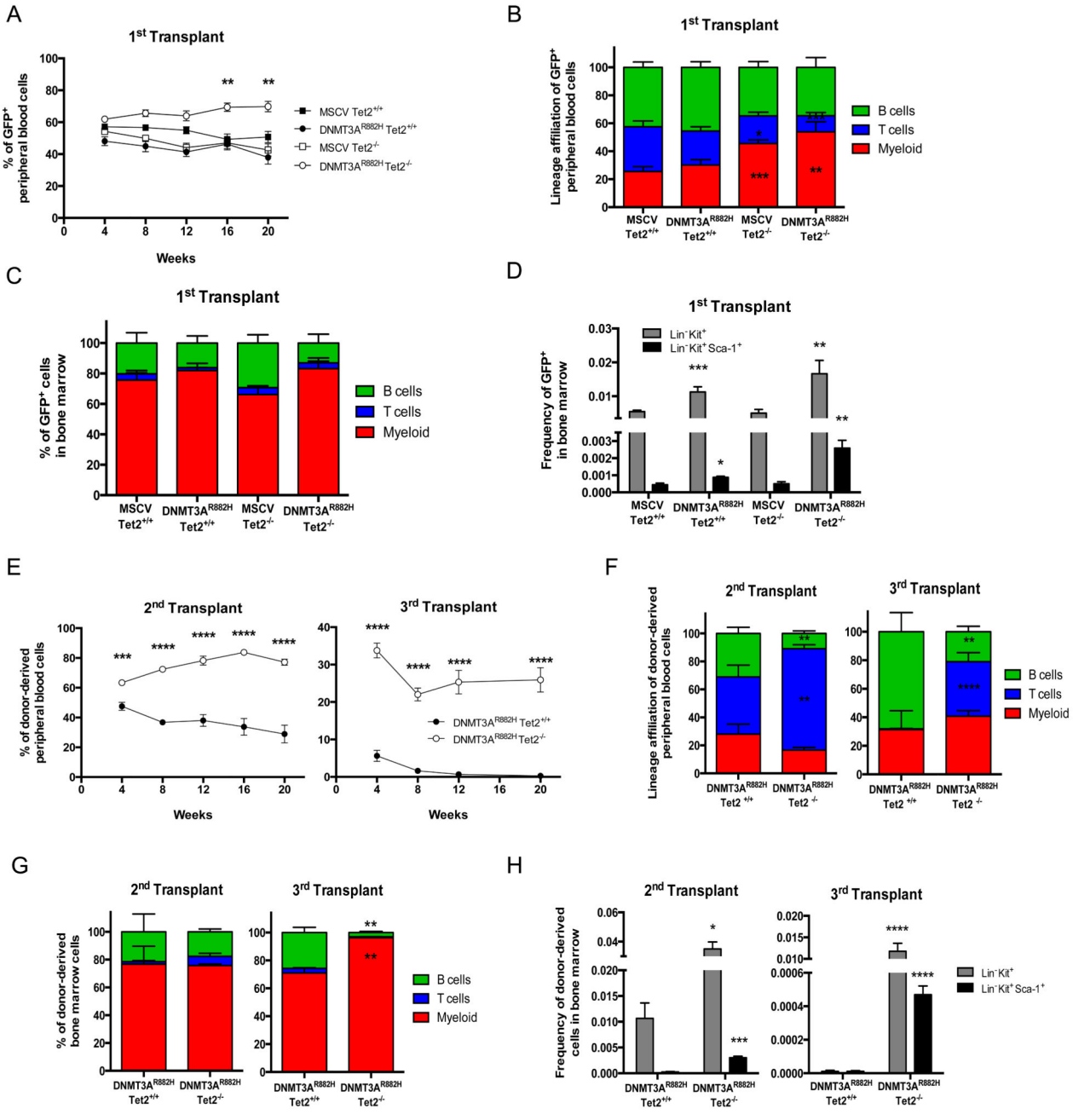

Figure 1. Proliferative advantage and impaired differentiation potential of *DNMT3A*^{R882H} *Tet2*$^{-/-}$ HSPC

Contribution of 1^{ary} control (*MSCV Tet2*$^{+/+}$), *DNMT3A* mutated (*DNMT3A*^{R882H} *Tet2*$^{+/+}$), *Tet2*-inactivated (*MSCV Tet2*$^{-/-}$) and *DNMT3A* mutated and *Tet2*-inactivated (*DNMT3A*^{R882H} *Tet2*$^{-/-}$) GFP^{+} HSPC in first transplant to: (**A**) blood cells showing significant enrichment for GFP^{+} *DNMT3A*^{R882H} *Tet2*$^{-/-}$ after 16 weeks (n= 8 to 20 mice per group); to (**B**) mature blood lineages at 20 weeks post-transplantation (n = 10 per group) and (**C**) to lineages at 20 weeks post-transplantation in bone marrow of 1^{ary} transplanted

Europe PMC Funders Author Manuscripts

Europe PMC Funders Author Manuscripts

mice (n = 3 per group). Shown are percentages of GFP^+ myeloid cells ($Mac1^+$ $Gr1^+$), B cells ($CD19^+$ $B220^+$) and T cells ($CD4^+$ and $CD8^+$) (**D**) Frequencies of GFP^+ Lin^- Kit^+ and Lin^- Kit^+ $Sca\text{-}1^+$ progenitors in 1^{ary} recipient mice (n = 3 per group). (**E**) Contribution of donor-derived GFP^+ $CD45.2^+$ HSPC to blood cells in 2^{ary} (n = 9) and 3^{ary} (n = 10) transplanted mice after 16 weeks. (**F**) Lineages contribution of GFP^+ HSPC at 20 weeks post-transplantation in blood in 2^{ary} and 3^{ary} transplanted mice (n = 7). (**G**) Lineage contribution of GFP^+ HSPCs at 20 weeks post-transplantation in bone marrow in 2^{ary} and 3^{ary} transplanted mice (n = 3). (**H**) Frequencies of GFP^+ Lin^- Kit^+ and Lin^- Kit^+ $Sca\text{-}1^+$ progenitors in 2^{ary} and 3^{ary} transplanted mice (n = 3). Mean ± SEM values are shown in graphs. An unpaired Student's *t* test was used for statistical analyses. Significant differences in comparison to *MSCV Tet2*$^{+/+}$ (figure 1B-D) and *DNMT3A*^{R882H} *Tet2*$^{+/+}$ (figure 1E-H) are indicated with *$p< 0.05$; **$p< 0.01$; ***$p< 0.001$; ****$p< 0.0001$.

Europe PMC Funders Author Manuscripts

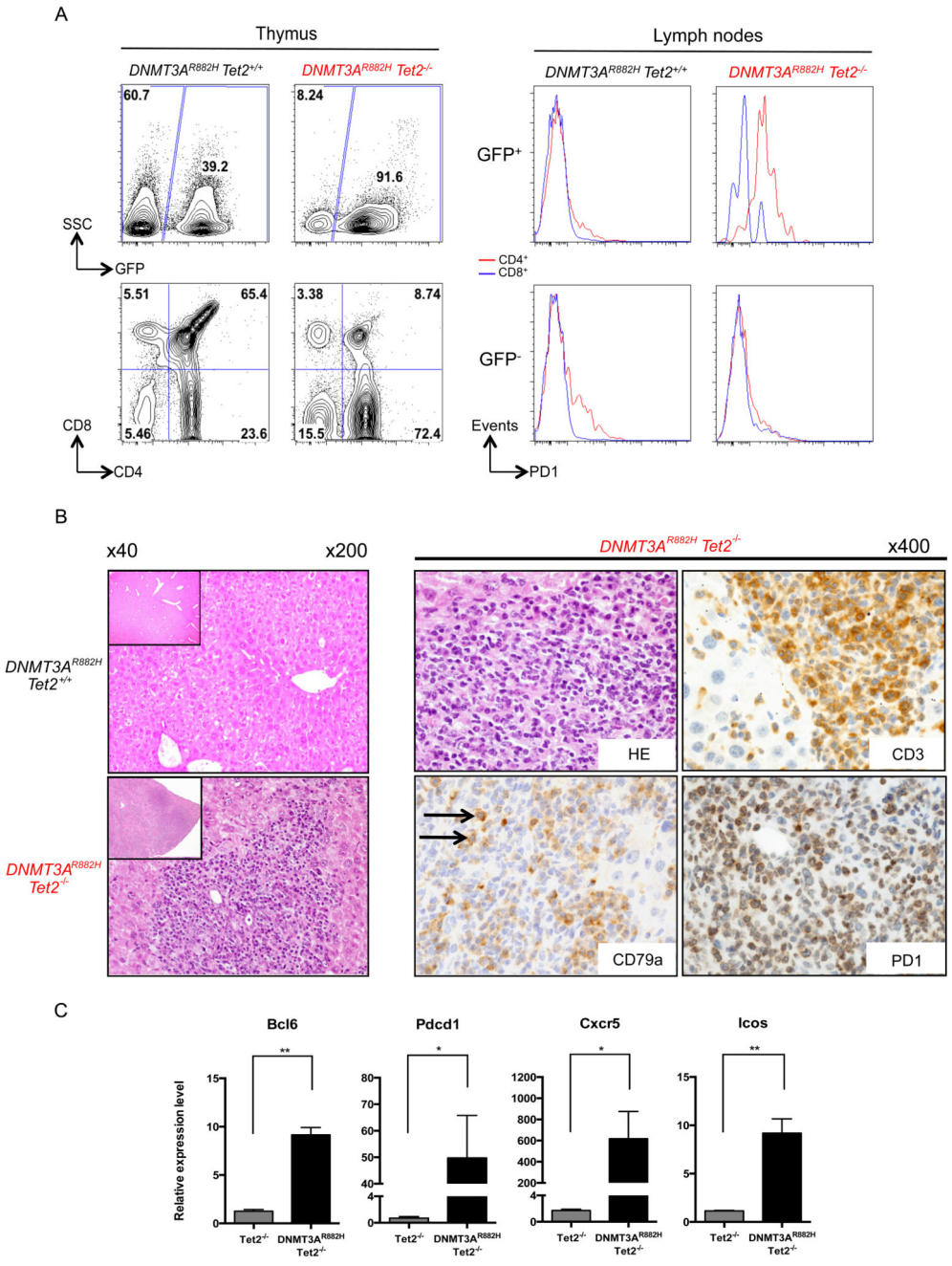

Figure 2. Development of AITL-like disease in mice serially transplanted with *DNMT3A*^{R882H} *Tet2*$^{-/-}$ HSPC

(**A**) Flow cytometry analysis of the thymic and nodal cells from 2^{ary} recipient mice. Frequencies of donor-derived GFP^{+} cells are represented (top, left). CD4^{+} population is expanded in the GFP^{+} fraction of *DNMT3A*^{R882H} *Tet2*$^{-/-}$ in comparison to *DNMT3A*^{R882H} *Tet2*$^{+/+}$cells (bottom, left). Analysis of nodal cells of 2^{ary} recipient mice show surface expression of PD1 in *DNMT3A*^{R882H} *Tet2*$^{-/-}$ GFP^{+} CD4^{+} (red) but not in CD8^{+} (blue) cells (top, right). GFP^{-} cells are shown as controls (bottom, right) (**B**) Hematoxylin-Eosin staining of liver sections from a 10 months symtomatic *DNMT3A*^{R882H} *Tet2*$^{-/-}$ (bottom,

left) animal and a *DNMT3A*^{R882H} *Tet2*$^{+/+}$ (top, left) control (original magnification 200). Insets show a smaller magnification of the same section and highlight the disorganized liver structure (original magnification 40). Pathological analysis of liver section from a symptomatic *DNMT3A*^{R882H} *Tet2*$^{-/-}$ mouse with Hematoxylin-Eosin (top, middle) showing a dense atypical lymphoid infiltrate, containing a prominent CD3^{+} T-cell population (top, right) expressing PD1 (bottom, right) admixed with scattered CD79a^{+} B-cells and plasmocytes (bottom, middle) (original magnification 400). Arrows point at scattered large B-cells recruited around T cells. (**C**) qRT-PCR validation of *Bcl6*, *Pdcd1*, *Cxcr5* and *Icos* genes overexpression in GFP^{+} CD4^{+} of AITL mice (n = 2) as compared to CD4^{+} *Tet2*$^{-/-}$ thymocytes (n = 3). Each value represents the mean ± SEM. An unpaired Student's *t* test was used for statistical analyses. Significant differences between groups are indicated *p< 0.05; **p< 0.01; ***p< 0.001; ****p< 0.0001.

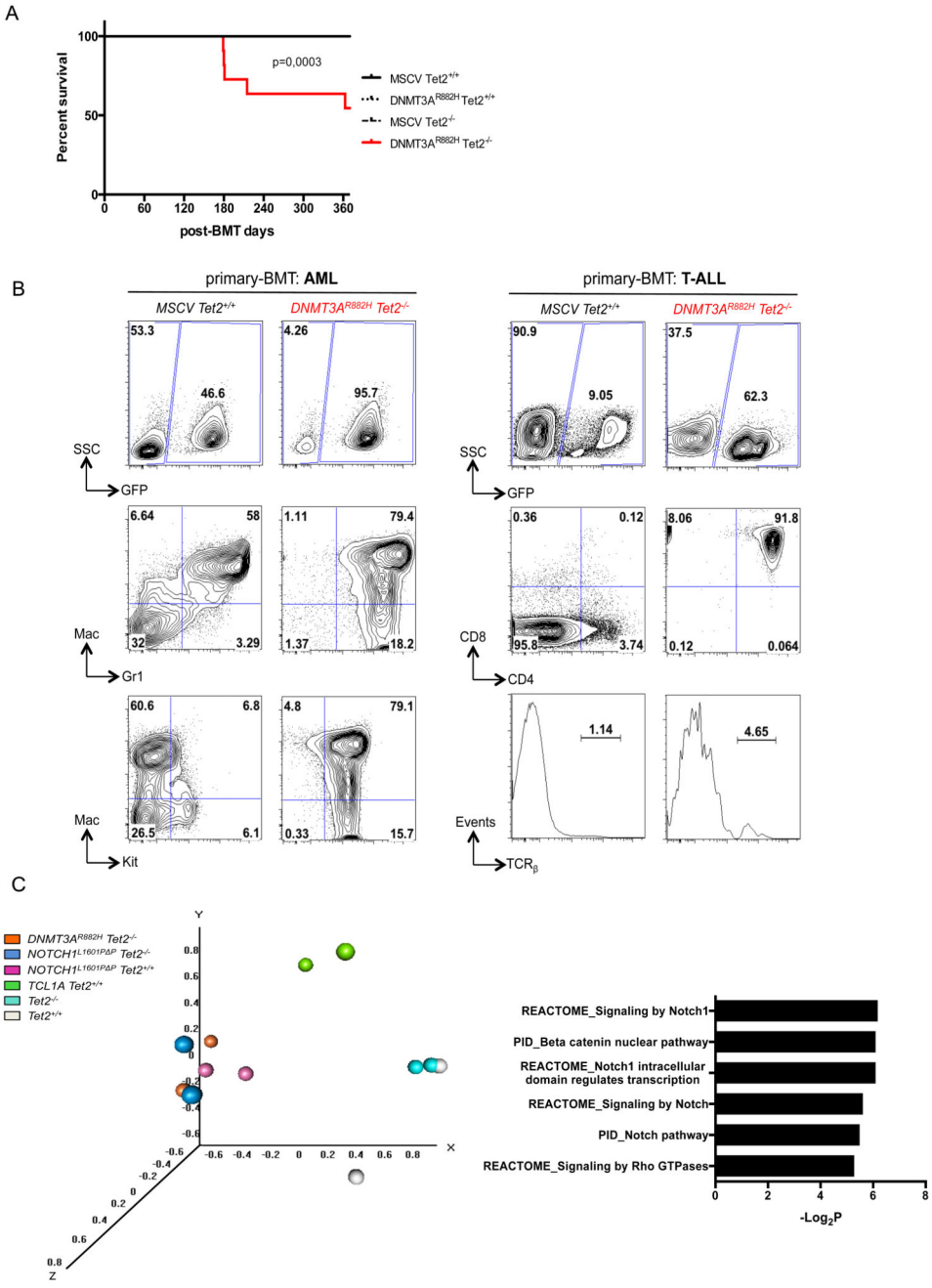

Figure 3. Development of acute leukemia in mice transplanted with *DNMT3A*^{R882H} *Tet2*$^{-/-}$ HSPC

(A) Kaplan-Meier survival curve of 1^{ary} control (*MSCV Tet2*$^{+/+}$), *DNMT3A* mutated (*DNMT3A*^{R882H} *Tet2*$^{+/+}$), *Tet2*-inactivated (*MSCV Tet2*$^{-/-}$) and *DNMT3A* mutated and *Tet2*-inactivated (*DNMT3A*^{R882H} *Tet2*$^{-/-}$) mice (n = 8 to 15 per group). (**B**) Representative flow cytometry analysis of bone marrow of a 1^{ary} recipient control and an AML mouse (left). Top, percentage of GFP^{+} cells, middle, Mac1^{+} and Gr1^{+} expression in GFP^{+} cells showing myeloid populations and bottom, Kit^{+} expression in GFP^{+} populations are

represented. Flow cytometry analysis of bone marrow of a 1^{ary} recipient control and a T-ALL mouse are represented as well (right). Top, percentage GFP^+, middle, $CD4^+$ and $CD8^+$ expression in GFP^+ cells were further gated showing T-lymphoid cells invasion. Bottom, TCR_β expression in total GFP^+ population is represented (**C**) Principal component analysis of expression profile from T-ALL samples compared to *Tet2*$^{-/-}$ and *Tet2*$^{+/+}$ thymocytes (left) and pathways analyses of genes differentially expressed between *DNMT3A*^{R882H} *Tet2*$^{-/-}$ T-ALL and *Tet2*$^{+/+}$ thymocytes (right). Complete list provided in Table S2.

Europe PMC Funders Author Manuscripts

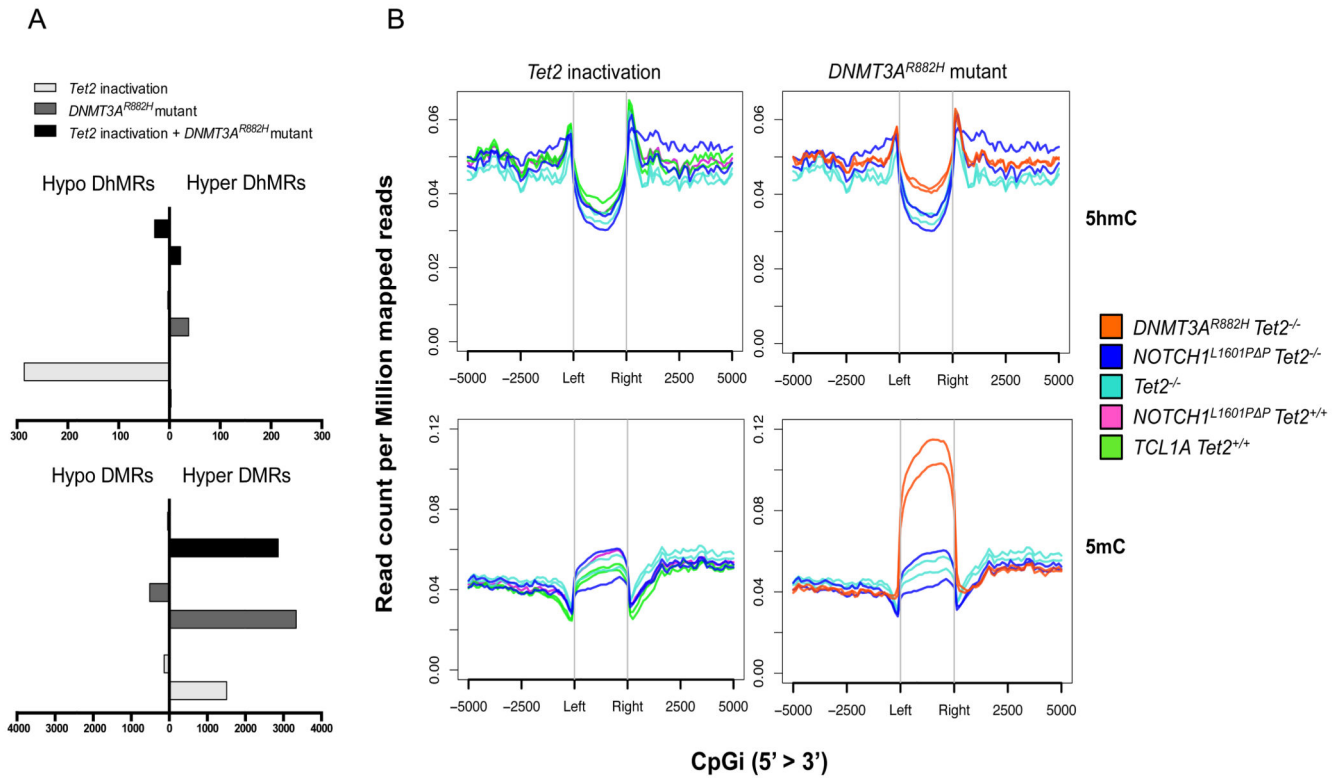

Figure 4. Genome-wide methylation and hydroxymethylation changes in tumoral *DNMT3A*^{R882H} *Tet2*$^{-/-}$ cells

(A) Number of differentially hydroxymethylated regions (DhMRs) (top) and differentially methylated regions (DMRs) (bottom) upon *Tet2*-inactivation, *DNMT3A*^{R882H} expression and compound *Tet2*-inactivation with *DNMT3A*^{R882H} mutant expression. (**B**) Normalized CpGi centered tag density profiles for 5-hmC (top) and 5-mC (bottom) ± 5kb flanking regions upon *Tet2*-inactivation (left) and *DNMT3A*^{R882H} mutant expression (right). This plot represents the frequency of 5-(h)mC on CpGi among the several T-ALL genotypes and highlights both a hypo-hydroxy and hypermethylation for *DNMT3A*^{R882H} *Tet2*$^{-/-}$ samples. Two replicates per genotype were used.

Europe PMC Funders Author Manuscripts

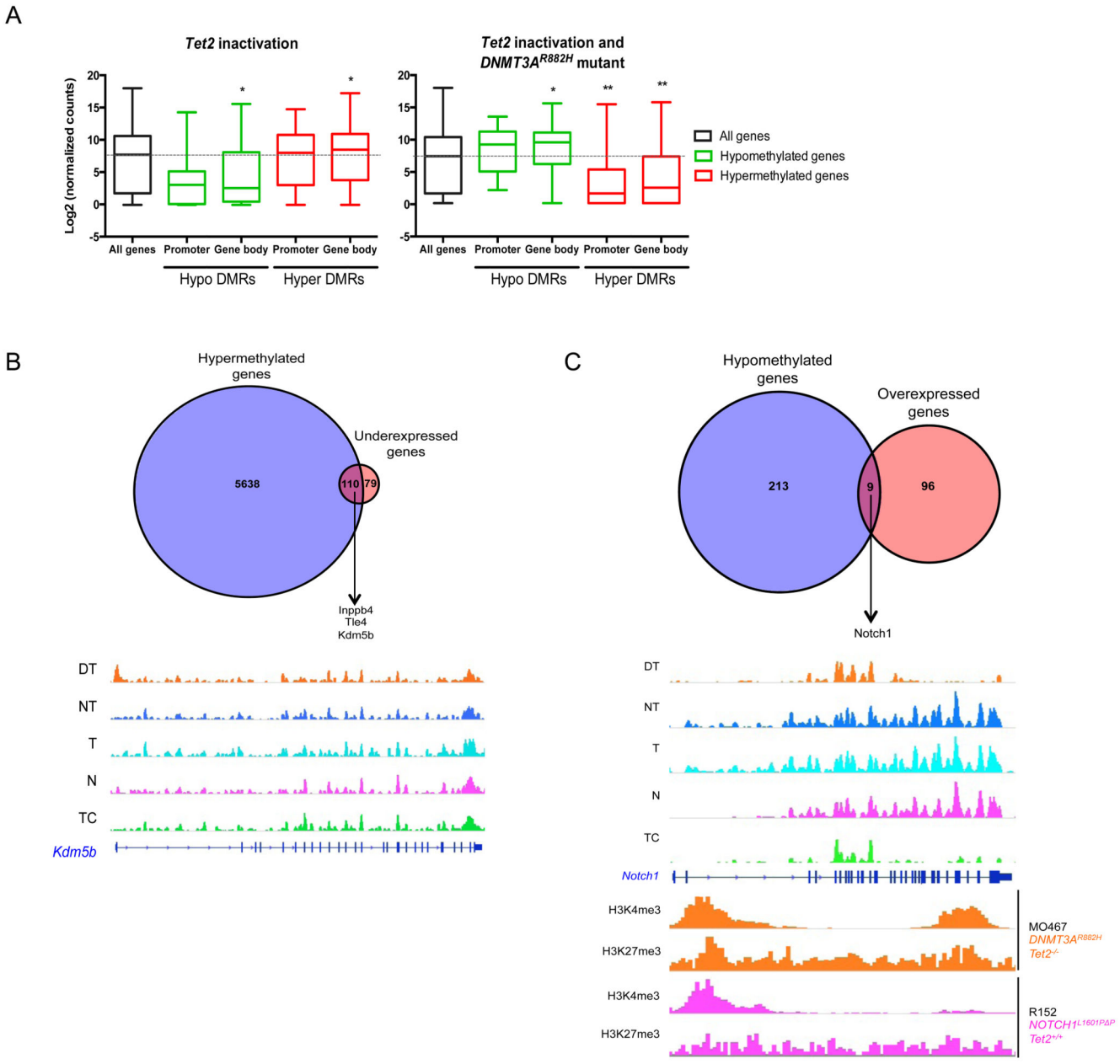

Figure 5. Correlation between methylation and transcriptional profiles of *DNMT3A*^{R882H} *Tet2*$^{-/-}$ tumoral cells

(**A**) Correlation between methylation on promoters or gene bodies and gene expression profiles associated with *Tet2*-inactivation (left), and both *Tet2*-inactivation and *DNMT3A*^{R882H} mutant expression (right). Significant differences in comparison to all genes are shown * 5e-02 < p > 1e-10; ** 1e-10 < p > 1e-100; *** p < 1e-100. (**B**) Venn diagram showing hypermethylated and underexpressed genes associated with *Tet2*-inactivation and *DNMT3A*^{R882H} mutant (top) and *Kdm5b* promoter hypermethylation in *DNMT3A*^{R882H} *Tet2*$^{-/-}$ sample (bottom). Methylation profiles of others T-ALLs and *Tet2*$^{-/-}$ non-transformed cells are used as controls (Table S1) (**C**) Venn diagram showing

Europe PMC Funders Author Manuscripts

hypomethylated and overexpressed genes associated with *Tet2* inactivation and $DNMT3A^{R882H}$ mutant (top) and *Notch1* gene body hypomethylation in $DNMT3A^{R882H}$ $Tet2^{-/-}$ sample (bottom). Methylation profiles of others T-ALLs and $Tet2^{-/-}$ non-transformed cells are used as controls (Table S1). Representative ChIPseq H3K4me3 and H3K27me3 marks performed on $DNMT3A^{R882H}$ $Tet2^{-/-}$ cell line MO467 showing gain of H3K4me3 mark in gene body region of *Notch1* locus, as compared with $Notch1^{L1601P\Delta P}$ $Tet2^{+/+}$ cell line R152. DT= $DNMT3A^{R882H}$ $Tet2^{-/-}$, NT= $NOTCH1^{L1601P\Delta P}$ $Tet2^{-/-}$, T= $Tet2^{-/-}$, N= $NOTCH1^{L1601P\Delta P}$ $Tet2^{+/+}$, TC= *TCL1A* $Tet2^{+/+}$, WT= $Tet2^{+/+}$ (Table S1).

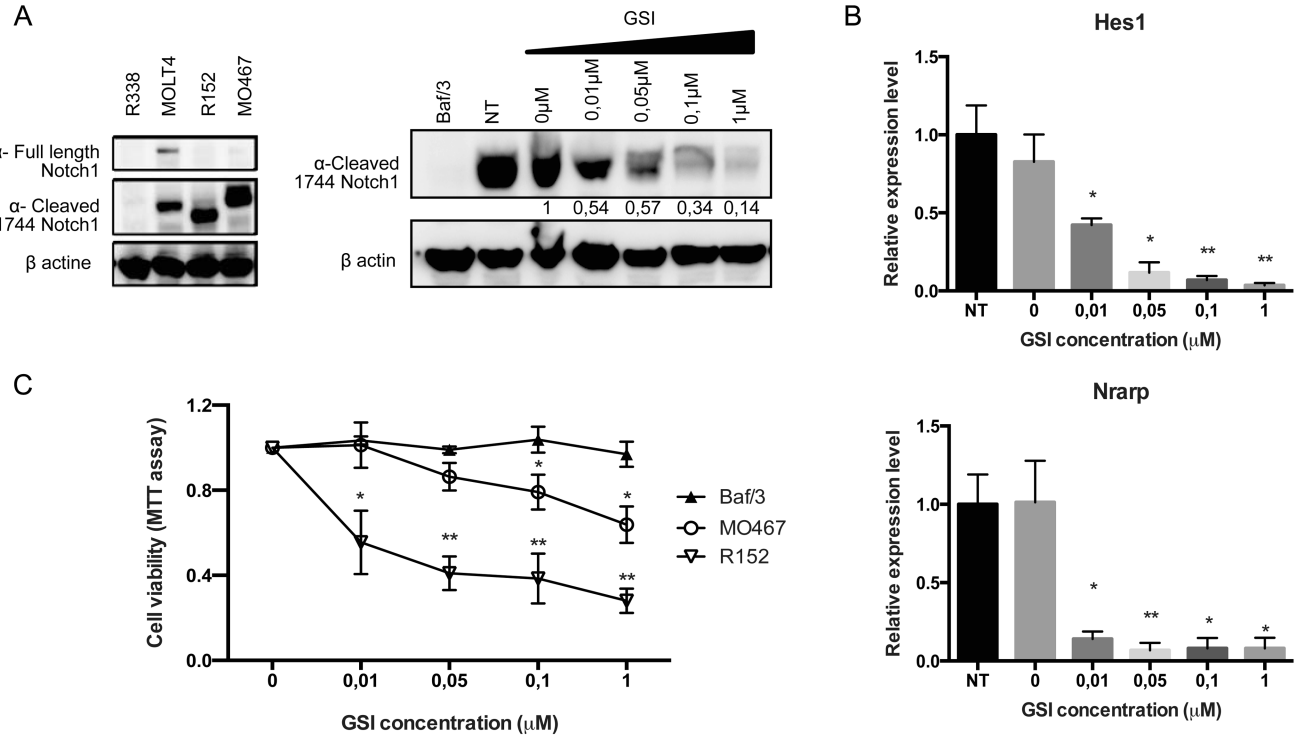

Figure 6. Notch dependency of tumoral *DNMT3A*^{R882H} *Tet2*$^{-/-}$ cells

(**A**) Notch1 full length or cleaved protein levels in murine *DNMT3A*^{R882H} *Tet2*$^{-/-}$ cell line MO467 show no full-length Notch1 protein as well as in *Notch1* $^{L1601P\Delta P}$ *Tet2*$^{+/+}$ cell line R152 (left). The human T-ALL cell line MOLT4 is used as a positive control and the murine T-ALL cell line R338 (from a *Ezh2*-deficient background) is used as a negative control. Notch1 cleaved protein levels in murine *DNMT3A*^{R882H} *Tet2*$^{-/-}$ cell line MO467 show a reduction of protein level among increasing amount of γ-secretase inhibitor doses (right). The murine cell line Baf/3 is used as a negative control. GSI = Gamma secretase inhibitor. (**B**) qRT-PCR validation of selected *Notch1* target genes *Hes1* (top) and *Nrarp* (bottom) downregulation upon γ-secretase inhibitor treatment during 48h. NT= non-treated. Each value represents the mean ± SEM (n = 3) of three independent experiments. (**C**) MTT assay on murine *DNMT3A*^{R882H} *Tet2*$^{-/-}$ cell line MO467 treated during 48h with increasing amount of γ-secretase inhibitor. The murine Baf/3 cell line is used as a negative control and the murine *Notch1*$^{L1601P\Delta P}$ *Tet2*$^{+/+}$ cell line R152 is used as a positive control. Each value represents the mean ± SEM (n = 3) of three independent experiments. Significant differences in comparison to Baf/3 cells are indicated *p< 0.05; **p< 0.01.

Europe PMC Funders Author Manuscripts

Table 1

Characteristics of symptomatic (AITL) and moribund (T-ALL and AML) mice

Survival indicates the number of survival days referring to subsequent transplant. Hemoglobin (HB) levels, white blood cell (WBC), red blood cell (RBC) and platelet (PLT) counts are indicated. Infiltration of tissues by GFP^+ lymphoid $CD4^+$ $CD8^+$, myeloid $Mac1^+$ $Gr1^+$ Kit^+ tumoral of GFP^+ $CD4^+$ $PD1^+$ populations was determined by flow cytometry.

Frequence	Round of transplantation	Survival (days)	WBC (Kcells/µL)	HB (g/dL)	RBC (Kcells/µL)	PLT (Kcells/µL)	GFP^+ tumoral population	Disease	Autopsy
5/18	1^{ary}	179	12,73	10,9	6,95	155	$Mac1^+$ $Gr1^+$ Kit^+	AML	Hepatosplenomegaly adenopathy
		180	8,15	13	8,77	723	$Mac1^+$ $Gr1^+$ Kit^+	AML	Hepatosplenomegaly adenopathy
		181	8,21	12,6	9,21	689	$CD4^+CD8^+$	T-ALL	Thymoma
		215	1,47	15	10,08	547	$CD4^+CD8^+$	T-ALL	Mediastinal tumor
		363	4,08	14,9	6,64	456	$CD4^+$ $PD1^+$	AITL	Hepatosplenomegaly adenopathy
4/6	2^{ary}	302	5,45	14,2	5,91	497	$CD4^+$ $PD1^+$	AITL	Splenomegaly adenopathy
		302	3,49	14,5	7,96	449	$CD4^+$ $PD1^+$	AITL	Splenomegaly adenopathy
		462	10,55	2,8	1,57	52	$CD4^+$ $PD1^+$	AITL	Splenomegaly adenopathy
		497	3,42	10,2	5,12	204	$CD4^+$ $PD1^+$	AITL	Splenomegaly adenopathy
5/6	3^{ary}	416	5,21	9,8	4,99	152	$CD4^+$ $PD1^+$	AITL	Splenomegaly adenopathy
		461	3	11,4	5,28	253	$CD4^+$ $PD1^+$	AITL	Splenomegaly adenopathy
		491	5,95	11,7	5,72	855	$CD4^+$ $PD1^+$	AITL	-
		491	1,93	12,8	6,41	866	$CD4^+$ $PD1^+$	AITL	Enlarged thymus
		491	4,27	13,3	6,25	793	$CD4^+$ $PD1^+$	AITL	-